PAPER REFERENCE: Q-VIII.2

CONTROL OF MOLECULAR EXCITATIONS IN NANOTUBE-HETEROSTRUCTURE TRANSISTORS

Per Hyldgaard[1]

Department of Applied Physics, Chalmers University of Technology and Göteborg University, S-412 96 Göteborg, Sweden

Abstract

Current-induced molecular excitations play an important role in molecular-electronics devices like the resonant-tunneling nanotube-heterostructure transistor [*Solid State Comm.* **116**, 569 (2000), *Science* **293**, 76 (2001)]. The nonlinear transport through a resonant level stimulates local molecular vibrations because the single-electron injection modifies the chemical bonding. I report and interpret out-of-equilibrium Green-function calculations to predict the resulting current-induced molecular stimulation as a function of the excitation frequency, the applied bias, and the electrostatic-gate potential. I show that the out-of-equilibrium operating conditions voids the traditional (detailed-balance) transition rules (relating spontaneous and stimulated emission/absorption). Finally, I show that the out-of-equilibrium results for the current stimulation permit a frequency-selective excitation of the nanotube vibrations.

Keywords: nanotube transistor, transport, current-induced molecular vibrations.

[1]Tel. +46 31 772 8422; Fax: +46 31 772 8426; E-mail: `hyldgaar@fy.chalmers.se`

1. Introduction

Fullerene nanotubes [1] show great promise for future nanoelectronics applications. The chiral structure [2] controls the nature of electronic conduction — metallic versus semi-conducting — and fullerene materials offer possible realization of the full range of molecular-electronics devices. The formation of nanotube heterostructures offers the realization of, *e.g,* single-junction (current-rectifying) diodes [3] and the nanoscale (double-junction) resonant-tunneling transistors, Fig. 1 [4, 5, 6]. The resonant-tunneling design [4, 6] was proposed [4] for the new nanotube transistor to ensure a robust, high-temperature device operation [7] which is insensitive to general elastic/inelastic scattering processes [4, 7, 8, 9]. However, a successful future molecular-electronics technology will require a more general understanding of both nanoscale electronic and nanoscale electron-mechanical devices [10]. For the electronics devices there is also a need to achieve an effective characterization of the atomic dynamics under the out-of-equilibrium conditions that define their operation. Here I report a nonequilibrium Green-function calculation of the current-induced molecular excitations, document a possible control, and suggest an in-situ probe [11, 12] of the dynamics in the nanotube-heterostructure transistor.

Fig. 1 illustrates the structure and operation of the robust nanotube-heterostructure transistor. In short, the nanotube-heterostructure transistor relies on a traditional field-effect control but replaces the semi-classical transport with resonant tunneling through molecular orbitals which are confined to the barrier region. For a sample realization at $L_{\rm B} = 3$ nm we have combined density-functional, electro-dynamical, and out-of-equilibrium Green-function calculations to characterize the resonant-tunneling transistor effect [4, 7]. Assuming a close position of metallic-nanotube gates we thus predict large tunneling rates $\Gamma_{\rm L/R} \approx 10$ meV and that a gate voltage $\Phi_{\rm gate} \sim 2$ V can enable a strong load current (drain-to-source)

$$J \leq J_{\rm RT} \equiv \left(\frac{e}{\hbar}\right) \frac{4\Gamma_{\rm L}\Gamma_{\rm R}}{\Gamma_{\rm L}+\Gamma_{\rm R}} \sim 5\ \mu{\rm A}, \tag{1}$$

while the (gate-to-source) input current remains vanishing $J_{\rm in} \ll 1$ nA. At low temperatures the tunneling current [8]

$$J(E_{\rm orb}(\Phi_{\rm gate});\mu_{L/R}) = J_{\rm RT}\,[P_{\rm occ}^{\mu_L}(E_{\rm orb}) - P_{\rm occ}^{\mu_R}(E_{\rm orb})], \tag{2}$$

can be described as a difference between occupation-probabilities

$$P_{\rm occ}^{\mu_{\rm L/R}}(E_{\rm orb}) \equiv \frac{1}{2} + \frac{1}{\pi}\arctan\left(\frac{\mu_{\rm L/R} - E_{\rm orb}}{\Gamma}\right). \tag{3}$$

The resonant-tunneling transistor supports fast (THz and beyond) operation because the gate control [7] remains possible and the transport robustness [8] remains valid at such frequencies. The resonant-tunneling transistor, Fig. 1, can also be realized by starting with an all-semiconducting nanotube and then locally modifying the conduction properties, for example, by a spatially varying electrostatic field [6]. To realize the robust resonant-tunneling transistor design [4] it is important only that the central nanoscale region (a) represents a conduction barrier, and (b) traps a set of well-resolved transport resonances. The predicted transistor robustness [4] ensures a partial insensitivity towards choice of such fabrication methods by suppressing the transport effects of defect scattering [7].

3. Theory of current-induced molecular excitation

The local molecular excitation $N_{\rm vib}(\Omega_i)$ of mode Ω_i is specified by a competition between the current-induced vibration-transition rates, $R_{\rm sp}$ and $R_{\rm ab}$, and the intrinsic decay rate $1/\tau_i$ arising through nanostructure-phonon decay or transport [11, 13, 14]:

$$(1/\tau_i)\,\delta N_{\rm vib}(E_{\rm orb}(\Phi_{\rm gate});\Omega_i) = R_{\rm sp}(E_{\rm orb};\Omega_i) - R_{\rm ab}(E_{\rm orb};\Omega_i)\delta N_{\rm vib}(E_{\rm orb}(\Phi_{\rm gate});\Omega_i). \tag{4}$$

The two current-induced transition rates, $R_{\rm sp}$ and $R_{\rm ab}$, describe the spontaneous (vibration/phonon) emission and net absorption, respectively. As indicated, these out-of-equilibrium transition rates $R_{\rm sp,ab}$ — and hence the local molecular excitation $\delta N_{\rm vib}$ — depend on the resonant-level energy position which in turn can be controlled by the potential $\Phi_{\rm gate}$ on an electrostatic gate.

This gate control, $R_{\rm sp}(E_{\rm orb}(\Phi_{\rm gate});\Omega_i)$ and $R_{\rm ab}(E_{\rm orb}(\Phi_{\rm gate});\Omega_i)$, is frequency selective and affected by the out-of-equilibrium electron distribution. An earlier paper [12] provided a formal calculation of $R_{\rm sp}$ and $R_{\rm ab}$ based on nonequilibrium Green functions [8]. For general electron-vibration matrix elements M_i the results, summarized below, are given to linear order in the coupling constants $g_i \equiv M_i^2/\Omega_i$.

The spontaneous vibration emission rate $R_{\rm sp}$ is given the excitation increase, $\delta N_{\rm vib}$, as one enables the current-vibration coupling, $g \to g \neq 0$. For slow phonon rate of decay, $\tau_i^{-1} \ll \Gamma$, the rate $R_{\rm sp}$ is then expressed as

$$\frac{R_{\rm sp}(E_{\rm orb};\Omega_i)}{gJ_{\rm RT}} = \frac{\Theta(\mu_L-\mu_R-\Omega_i)\Omega_i^2}{4(\Omega_i^2+4\Gamma^2)}\left[\Delta P_{\rm occ}(E_{\rm orb};\Omega_i)+\Delta P_{\rm log}(E_{\rm orb};\Omega_i)\right]. \qquad (5)$$

where

$$\begin{aligned}\Delta P_{\rm occ}(E_{\rm orb};\Omega_i) &= \left[P_{\rm occ}^{\mu_L}(E_{\rm orb})-P_{\rm occ}^{\mu_R}(E_{\rm orb}-\Omega_i)\right] \\ &+ \left[P_{\rm occ}^{\mu_L}(E_{\rm orb}+\Omega_i)-P_{\rm occ}^{\mu_R}(E_{\rm orb})\right], \qquad (6)\end{aligned}$$

while the logarithmic contribution $\Delta P_{\rm log}$ can be ignored [12] for the relevant case of $\Gamma \ll \Omega_i$. The rate $R_{\rm sp}$ is directly proportional to the out-of-equilibrium electron current $J_{\rm RT}$ but limited by the availability of phase space [12], $\Delta P_{\rm occ}(E_{\rm orb};\Omega_i)$.

The net vibration absorption is given by the retarded density-correlation function $\Pi_r^0(\Omega_i)$ evaluated for general out-of-equilibrium tunneling conditions in Ref. [9]. The rate $R_{\rm ab}$ is here evaluated at $\Omega_i \gg \Gamma$, yielding

$$\begin{aligned}\frac{R_{\rm ab}(E_{\rm orb};\Omega_i)}{gJ_{\rm RT}} &= \frac{-{\rm Im}\,\Pi_r^0(\Omega_i)\,\Omega_i^2}{J_{\rm RT}} \approx \frac{\Gamma\Omega_i^2}{4(\Omega_i^2+4\Gamma^2)} \times \\ &\Big(\Gamma_{\rm R}^{-1}\left[P_{\rm occ}^{\mu_L}(E_{\rm orb}-\Omega_i)-P_{\rm occ}^{\mu_L}(E_{\rm orb}+\Omega_i)\right] \\ &+ \Gamma_{\rm L}^{-1}\left[P_{\rm occ}^{\mu_R}(E_{\rm orb}-\Omega_i)-P_{\rm occ}^{\mu_R}(E_{\rm orb}+\Omega_i)\right]\Big). \qquad (7)\end{aligned}$$

where, again, one can ignore a negligible logarithmic correction [9, 12]. The result (7) taken together with causality, $-{\rm Im}\Pi_{\rm r}^0 > 0$, constitute proof that a single resonant-level transport system can *never* support a net stimulated (vibration/phonon) emission, $R_{\rm ab} \sim -{\rm Im}\,\Pi_{\rm r}^0 > 0$.

I stress that the traditional Einstein relation [15], $R_{\rm sp} \equiv {\rm const}\times R_{\rm ab}$, does not apply here because there is no detailed balance in the presence of current injection. The net stimulated absorption rate $R_{\rm ab}$ is defined by a different phase-space measure (7) than the measure (6) that defines $R_{\rm sp}$. In contrast to Eq. (6), the $R_{\rm ab}$ phase space, Eq. (7), involves differences of contributions, Eq. (3), evaluated at the *same* chemical potential (at $\mu_{\rm L}$ or $\mu_{\rm R}$). It is thus possible to provide an independent, frequency-selective control of $R_{\rm sp}(E_{\rm orb};\Omega_i)$ and $R_{\rm ab}(E_{\rm orb};\Omega_i)$.

4. A nanotube-heterostructure molecular-dynamics probe

The left-most top and bottom panels of Fig. 2 contrast the independent gate-voltage control of the electron-vibration interaction effects in $R_{\rm sp}$ and $R_{\rm ab}$ for two optical modes Ω_0 (solid curve) and Ω_1 (dashed curve). For the nanotube-heterostructure transistor [4, 5], it is relevant to consider the current-induced excitation at energies Ω_i = 100–200 meV. I concentrate on a pair of high-energy modes, at assumed frequencies $\Omega_{1(0)}$ = 200 meV (120 meV) $\gg \Gamma$, assume a fixed applied bias $\mu_L - \mu_R$ = 300 meV, and describe the current stimulation at zero temperature to discuss the formal results and predictions, Fig. 2 & 3. The gate voltage $\Phi_{\rm gate}$ adjusts the resonant energy position, $E_{\rm orb}(\Phi_{\rm gate}) - \mu_{\rm L}$, and provides the implicit gate control shown in the pair of panels. The excitation transition rates are here illustrated for equal electron tunneling rates, $\Gamma_{\rm L} = \Gamma_{\rm R}$. A qualitatively different control of the current-induction transition rates arises within the region, $\mu_{\rm L} > E_{\rm orb} > \mu_{\rm R}$ (identified by vertical dotted lines), when the electrostatic gate enables a strong resonant-tunneling current, Eq. (2).

The frequency-selective control of out-of-equilibrium transition rates results from differences in the Pauli-exclusion effects on the $R_{\rm sp}$ and $R_{\rm ab}$ transition phase space (6) and (7). The four right-most panels, A, C_0, C_1, & B, of Fig. 2 detail, for $J\sim J_{\rm RT}$, the differences in transport conditions, electron occupation, and hence phase-space restrictions that define the independent gate-control of $R_{\rm sp}$ and $R_{\rm ab}$ for the frequencies $\Omega_{0,1}$. In these four panels the thick line identifies the (gate-controlled) energy position of the resonant level; the set of two thin solid (dashed) lines identifies the energy position of the pair of vibration satellites $E_{\rm orb}\pm\Omega_0$ ($E_{\rm orb}\pm\Omega_1$.)

In the schematics, one or two downward arrow(s) $r_{\rm sp}$ identify conditions when the current flow causes a spontaneous emission of a molecular vibration as permitted by the Pauli exclusion principle. This Pauli-exclusion control of the spontaneous emission processes reflects directly the phase-space measure, Eq. (6). Specifically, in region A (B) this emission arises when an electron tunnels into $E_{\rm orb}$ (into $E_{\rm orb}+\Omega_{i=0,1}$) but leaves at energy $E_{\rm orb}-\Omega_{i=0,1}$ (at $E_{\rm orb}$). For an applied bias which satisfies $2\Omega_1 > eV_{\rm bias} > \Omega_1$ (panel C_1) neither type-A nor type-B vibration-emission processes are possible for local mode Ω_1. *However,* both types of spontaneous emission processes remain possible for a vibrational mode at $\Omega_0 < eV_{\rm bias}/2$ (panel C_0).

The presence of upwards arrows $r_{\rm ab}$ instead identifies conditions for a net current-induced absorption, $R_{\rm ab}\neq 0$. In section A (B) a net absorption arises when the electron enters at $E_{\rm orb}$ (at $E_{\rm orb}-\Omega_{i=0,1}$) but leaves at $E_{\rm orb}+\Omega_{0,1}$ (at $E_{\rm orb}$). Tuning $E_{\rm orb}$ to the central region C causes an enhanced absorption for mode Ω_1 as both type-A and type-B absorption processes become possible (panel C_1). *However,* for the lower mode at $\Omega_0 < eV_{\rm bias}/2$, I find an effective cancellation (panel C_0), as the energies $E_{\rm orb}$ and $E_{\rm orb}\pm\Omega_0$ all carry a partial electron occupation and thus produce a vanishing *net* absorption rate, $R_{\rm ab}\to 0$.

Frequency-selective molecular-vibration stimulation. Fig. 3 documents that an optimization of current-induced molecular excitation is possible. The figure contrasts the gate variation (Eq. (4)) of the molecular-excitation levels, $\delta N_{\rm vib}(\Omega_0)$ and $\delta N_{\rm vib}(\Omega_1)$, and details methods to enhance the current stimulation of mode Ω_0 at the expense of mode $\Omega_1 > \Omega_0$. Such selective excitation is possible even when $eV_{\rm bias} > \Omega_1 \gg \Gamma$, and arises when $2\Omega_1 > eV_{\rm bias} > 2\Omega_0$ and $E_{\rm orb}$ is tuned to region C ($E_{\rm orb}\approx(\mu_{\rm L}+\mu_{\rm R})/2$). These nonequilibrium transport conditions simultaneously minimize $R_{\rm st}(\Omega_1)$ and maximize the ratio $R_{\rm st}(\Omega_0)/R_{\rm ab}(\Omega_0)$ to extinguish $\delta N_{\rm vib}(\Omega_1)$, thus selectively enhancing the lower-frequency current stimulation $\delta N_{\rm vib}(\Omega_0)$.

In turn, such control could provide a novel frequency-selective and in-situ source of local molecular-transistor vibrations to probe the current-induced nanoscale molecular dynamics. The panel documents an implicit electrostatic gate control for the current stimulation $\delta N_{\rm vib}(\Omega_{0,1})$ arising through adjustments of the resonant-level energy position, $E_{\rm orb}(\Phi_{\rm gate})$ [7]. This control permits a switch between disabling and enabling the current-stimulation (4) and could thus produce a frequency-selective burst of molecular vibration, $\delta N_{\rm vib}(\Omega_0) \gg 0$. Nanoscale molecular-dynamics probing is then possible with simultaneous Raman measurements of the anti-Stokes signal at Ω_0 because the anti-Stokes strength is sensitive [16] to the excess molecular-excitation burst $\delta N_{\rm vib}(\Omega_0) \gg 0$. Such Raman measurements can through Eq. (4) determine the decay $1/\tau_i$ that characterizes these nanostructure molecular excitations and thus probe mechanisms [11, 13, 14] which determine the intrinsic nanoscale molecular dynamics.

5. Conclusions

For the resonant-tunneling heterostructure transistor [4, 5, 6]. I have calculated the current-induced molecular vibration and interpreted the results for both the (current-induced) spontaneous emission and for the net absorption. The out-of-equilibrium results differ from the traditional Einstein relations (which assume detailed balance). In addition, I show that it is possible to obtain a frequency-selective control of the nanotube-heterostructure molecular excitation and I propose a novel in-situ probe of the current-induced dynamics.

6. Acknowledgements

This work was supported by the W. & M. Lundgrens Foundation, and by the Swedish Foundation for Strategic Research (SSF) through ATOMICS.

References:

[1] C. Dekker, *Phys Today* **May 1999**, 22 (1999).

[2] C. T. White and J. W. Mintmire, *Nature* **394**, 29 (1998).

[3] Z. Yao, H. W. C. Postma, L. Balents, and C. Dekker, *Nature* **402**, 273 (1999).

[4] P. Hyldgaard and B. I. Lundqvist, *Solid State Comm.* **116**, 569 (2000).

[5] H. W. C. Postma, T. Teepen, Z. Yao, M. Grifoni, and C. Dekker, *Science* **293**, 76 (2001).

[6] F. Leonard and J. Tersoff, *Phys. Rev. Lett.* **88**, 258302 (2002).

[7] P. Hyldgaard and B. I. Lundqvist, *Mat. Science Eng. C* **19**, 445 (2002).

[8] J. H. Davies *et al, Phys. Rev. B* **47**, 4603 (1993).

[9] P. Hyldgaard, S. Hershfield, J. H. Davies, and J. W. Wilkins, *Annals of Physics,* **236**, 1 (1994).

[10] L. Y. Gorelik, A. Isacsson, M. V. Voinova, B. Kasemo, R. I. Shekhter, and M. Jonson, *Phys. Rev. Lett.* **80**, 4526 (1998).

[11] V. Narayanamurti, *Science* **213**, 717 (1981).

[12] P. Hyldgaard, *Low Temperature Physics* **27**, 585 (2001).

[13] S. G. Walkauskas, D. A. Broido, K. Kempa, and T. L. Reinecke, *J. Appl. Phys.* **85**, 2579 (1999); P. Hyldgaard and G. D. Mahan, *Thermal Conductivity* **23** (Technomic Publishing Company, Inc., Lancaster, Pennsylvania, 1996), p. 172.

[14] P. Hyldgaard and G. D. Mahan, *Phys. Rev. B* **56**, 10754 (1997).

[15] A. Einstein, *Phys. Zs.* **18**, 121 (1917).

[16] K. Kneipp, Y. Wang, H. Kneipp, I. Itzkan, R. R. Dasari, and M. S. Feld, *Phys. Rev. Lett.* **76**, 2444 (1996).

FIGURE CAPTIONS

Figure 1: Sample realization of the robust resonant-tunneling nanotube transistor [4, 5, 6]. A short, nanoscale L_B, section of non- or semi-conducting barrier (central region) inserted between a pair of metallic-nanotube leads (gray tubes) confines a (lowest-unoccupied) resonant orbital $\Psi_{\rm orb}$ of energy $E_{\rm orb}$. A pair of external contacts (triangles) maintain the leads at different chemical potentials $\mu_{\rm L/R}$. The barrier extension generally inhibits transport but a resonant-tunneling current, Eq. (1), arises when, e.g., $\mu_{\rm R} < E_{\rm orb} < \mu_{\rm L}$. This current is specified by resonance-to-lead tunneling rates $\Gamma_{\rm L/R}$ (arrows). A finite potential $\Phi_{\rm gate}$ at a close gate, e.g., a metallic nanotube, controls the electron potential inside the barrier region, adjusts the resonant-energy position $E_{\rm orb}(\Phi_{\rm gate})$, and provides the transistor operation.

Figure 2: Frequency-selective, independent gate control of the current-induced vibration/phonon spontaneous emission and net absorption rates, $R_{\rm sp}$ and $R_{\rm ab}$. The left-most top and bottom panels contrast the gate variation of the spontaneous phonon emission rate $R_{\rm sp}$ and net absorption rate $R_{\rm ab}$ at two frequencies $\Omega_{0,1}$. Both rates are proportional to $J_{\rm RT}$ and the electron-vibration coupling constant g. The gate variation is implicit and defined through $E_{\rm orb}(\Phi_{\rm gate})$. The set of four right-most panels illustrate the Pauli exclusion mechanism responsible for the frequency-selective control. Here the set of downward (upward) arrows labeled by $r_{\rm sp}$ ($r_{\rm ab}$) identify inelastic tunneling events that contribute to the spontaneous emission (to the net stimulated absorption).

Figure 3: Frequency selective current stimulation of molecular vibrations. The figure contrasts the current-induced increase in excitation levels, $\delta N_{\rm vib}(\Omega_0)$ (solid curve) and $\delta N_{\rm vib}(\Omega_0)$ (dashed curve) for a given intrinsic vibration decay time τ.

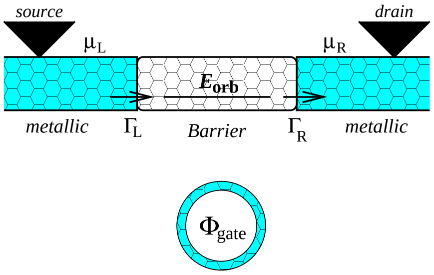

Figure 1

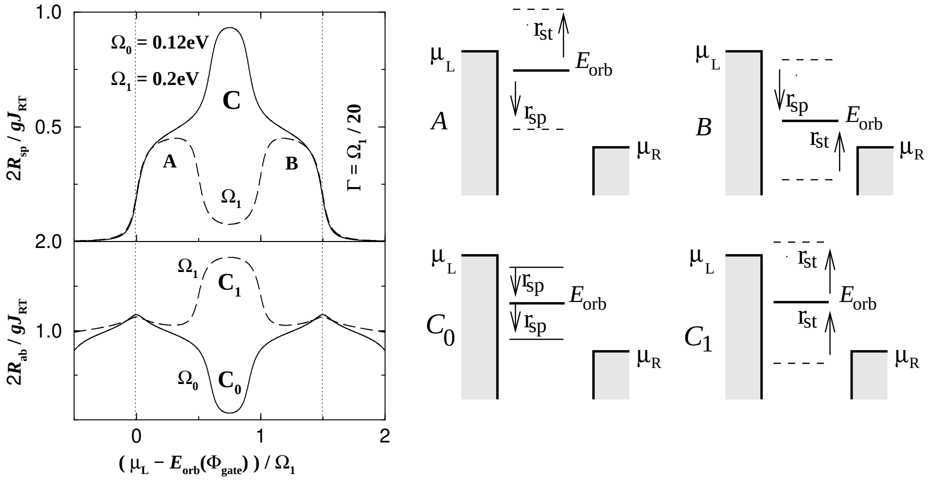

Figure 2

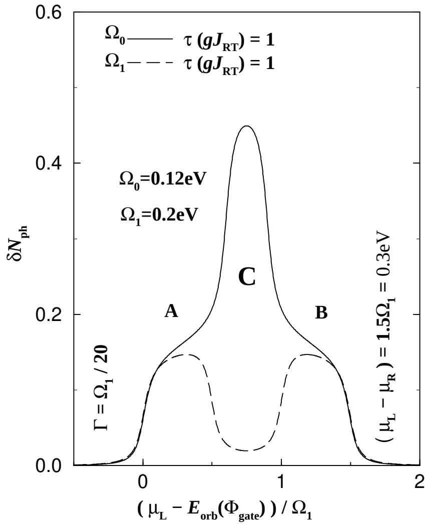

Figure 3